Multimode Balanced Mu-Near-Zero Loop Antenna for Wi-Fi 6/6E Applications in Full Metal Housing Tablet Computers

Wendi Yan, *Graduate Student Member, IEEE*, Yongjian Zhang, Kaifeng Li, Hui Lin, Heng Guo, Shumin Liao, and Yue Li, *Senior Member, IEEE*

***Abstract*— In this article, we introduce a balanced broadband mu-near-zero (MNZ) loop antenna, which is designed for Wi-Fi 6/6E applications in full metal housing tablet computers. Different from the previous MNZ segmented loop antenna with the single 0^{th} mode, the higher order $1^{st}/2^{nd}/3^{rd}$ modes are also included for broadband purpose. By adjusting the effective permeability through the distributed capacitors in the proposed antenna, the electrical lengths of the $0^{th}/1^{st}/2^{nd}/3^{rd}$ modes are reasonably stretched. This allows for multimode synergy in a single MNZ loop located in full metal housing computers. Therefore, the proposed MNZ loop antenna, with a planar structure of 6.8 × 45.4 mm^2, exhibits a broad bandwidth with $S_{11} < -6$ dB from 4.5 to 7.5 GHz, covering Wi-Fi 6/6E bands. As another merit for practical applications, this broadband MNZ loop antenna is also balanced with less current on the motherboard, performing excellent robustness against changes in tablet computer sizes or affecting by hands. The proposed MNZ loop antenna, with its multiple modes, offers valuable insights for the development of broadband and robust antennas in full metal housing devices.**

***Index Terms*— Broadband antennas, full metal housing, mobile antennas, mu-near-zero (MNZ) antennas.**

I. Introduction

AS AN important component of modern wireless mobile devices, tablet computers are used in various scenarios due to their portability and handwriting convenience. Among them, full metal housing architectures are highly favored by users due to the advantages of attractive appearance, efficient heat dissipation, rugged shell, and easy integration [1], [2], [3], [4]. The primary method for wireless communication in tablet computers is through Wi-Fi. The Wi-Fi 6 protocol standards cover the 2.4-GHz (2.4–2.484 GHz) and 5-GHz (5.13–5.83 GHz) bands. Wi-Fi 6E extends the band up to 6 GHz (5.925–7.125 GHz) to enhance communication bandwidth. Generally, mobile terminal antennas for Wi-Fi 6/6E applications require a −6-dB bandwidth ranging from 5.15 to 7.125 GHz and an efficiency above −5 dB, with no specific requirement for the radiation pattern. Therefore, it is of great significance to design broadband antennas in full metal housing tablet computers for Wi-Fi 6/6E applications.

In recent years, antennas used in terminals are widely investigated [2], [3], [5], [6], [7], [8], [9], [10], [11], [12], [13], [14], [15], [16], [17]. Antennas used in terminals with full metal housings can be categorized into three types, including invert-F antenna [2], [5], [6], monopole antenna [7], [8], and slot antenna [3], [9]. These antennas exhibit good performance in terms of size and bandwidth. However, both the invert-F and the monopole antennas require a connection to the motherboard, while the slot antenna requires the engraving of slots on the motherboard or metal housings. These approaches introduce unexpected currents to the motherboard or metal housings, resulting in frequency drift and reduced efficiency when influenced by users' heads or hands. To mitigate the impact of unexpected currents, the best approach is to use balanced antennas [18], [19], [20], [21], [22], [23], [24]. Three methods have been employed to construct the balanced antennas in terminals. The first method is to design balanced antenna structure, such as one-wavelength mode of loop antenna [20], [21]. The second method involves decoupling between the ground and unbalanced antenna [22], [23]. For example, the authors propose the balanced monopole antenna in [22] and the balanced slot antenna in [23] through the distinct decoupling structure design. The third method is to use mode transformers to design antenna from an unbalanced mode to a balanced mode. Sui et al. [24] introduce a T-shaped structure for this conversion, reaching a relative bandwidth of 14.1%. Currently, we have not found any work on designing balanced antennas in tablet computers with a full metal housing.

Among the balanced antennas, a common method to achieve broadband performance is multimode design [25], [26], [27], [28]. The mu-near-zero (MNZ) antenna, whose permeability can be adjusted approximately through loading capacitors, provides an approach to tune the wavelength of modes. However, the MNZ loop antennas in [25] and [26] only study the 0^{th} mode without considering the higher order modes. The MNZ dipole antennas in [27] and [28] realize mode compression

Manuscript received 4 January 2024; revised 16 April 2024; accepted 3 May 2024. Date of publication 17 May 2024; date of current version 9 July 2024. This work was supported by the National Natural Science Foundation of China under Grant U22B2016, in part by the National Key Research and Development Program of China under Grant 2021YFA0716601, and in part by Lenovo. *(Corresponding author: Yue Li.)*

Wendi Yan, Yongjian Zhang, Kaifeng Li, and Yue Li are with the Department of Electronic Engineering, Beijing National Research Center for Information Science and Technology, Tsinghua University, Beijing 100084, China (e-mail: lyee@tsinghua.edu.cn).

Hui Lin, Heng Guo, and Shumin Liao are with Tablet Business, Lenovo, Beijing 100193, China.

Color versions of one or more figures in this article are available at https://doi.org/10.1109/TAP.2024.3399931.

Digital Object Identifier 10.1109/TAP.2024.3399931

between the 1st mode and the 3rd mode, with a considerable size. MNZ antennas applied in terminals with higher order modes have not been studied yet.

In this article, we introduce a balanced broadband MNZ loop antenna, which is designed for Wi-Fi 6/6E applications in full metal housing tablet computers. Based on a segmented loop antenna structure, we demonstrate the multimode to realize broadband performance. Through adjusting the effective permeability of the MNZ loop antenna, the 0th/1st/2nd/3rd modes are reasonably coupled in the identical physical dimensions. Therefore, the multimode MNZ loop antenna with broadband property is realized, covering both 5 and 6 GHz of Wi-Fi 6/6E in a mock-up full metal housing tablet computer. The simulated bandwidth with $S_{11} < -6$ dB is 4.5–7.5 GHz, accounting for 50% of the central frequency, with a planar structure of 6.8×45.4 mm^2. The experimental results effectively validate the simulation results. Benefiting from the balanced mode, the proposed antenna exhibits robust performance affected by the different tablet sizes or by users' hands. The proposed MNZ antenna, with its multiple modes, holds significant instructive value for the design of broadband antennas in mobile terminals.

II. Antenna Configuration

Fig. 1 illustrates a universal tablet computer with a full metal housing, representing the application scenario for the proposed antenna. The tablet computer consists of three components, including a glass screen, a metal motherboard, and a full metal housing. Typically, the metal motherboard is connected to the metal back plate of the screen, which can be seen as a large piece of metal under the screen. The glass screen completely covers the top surface of the metal housing, leaving a clearance between the metal motherboard and the metal housing. The internal structures of real tablet computers are extremely complex, and there are significant differences among various types of computers structures, making it challenging to directly establish models. To simplify the analysis, we only retain the structures that have the greatest impact on the antenna performance, i.e., the metal motherboard and the metal housing, and create a mock-up environment for antenna design.

Fig. 2 illustrates the geometry of the proposed antenna in the mock-up environment. As depicted in Fig. 2(a), the mock-up scenario comprises three metallic parts, which have obvious impact on antenna performance, including the metal back cover, frame, and ground. Here, the back cover of the full metal housing in the tablet computer corresponds to the metal back cover in the mock-up sample, while the motherboard together with the metal back plate of the screen in the tablet computer corresponds to the metal ground in the mock-up sample. Furthermore, simulations have shown that the radiation performance of the proposed antenna is minimally affected by the presence or absence of the glass screen. Hence, to maintain the brevity of our article, we opt to omit the glass screen in the mock-up sample. The proposed antenna, based on a printed-circuit-board (PCB) technique, is situated in the clearance between the frame and the ground. The dimensions of the tablet computer are $l_b \times w_b$, and the clearance is d_c. Fig. 2(b) presents a detailed top view of the

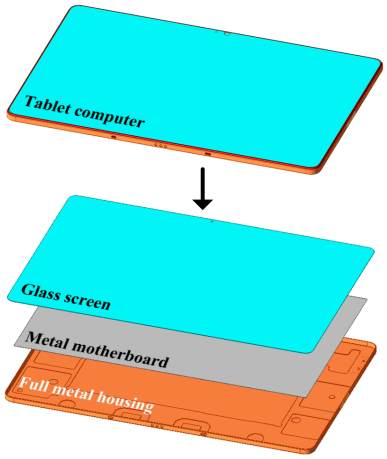

Fig. 1. Application scenarios of the proposed antenna in full metal housing tablet computer.

antenna structure. The segmented loop antenna has dimensions $l_a \times w_a$, with the thickness of t_a, placed at a position d_c from the right frame. Six gaps are left in the loop, serving as distributed capacitors. These gaps can be divided into two categories, with the middle two gaps labeled as w_{c1}, and the remaining four gaps as w_{c2}. These gaps are equidistant from each other, and the distances are equal to 1/6 of the entire loop circumference. A lumped port with 50 Ω is positioned centrally between the two leftmost capacitors, serving to excite various modes on the loop antenna. As depicted in Fig. 2(c), the overall tablet has a height of h_b. The thickness of both frames and back cover is t_d. The thickness of metal ground is t_g. The substrate, made of F4B with $\varepsilon_r = 2.65$ and $\tan\delta = 0.002$, has a thickness of t_d, and its top and bottom surfaces are aligned with the ground.

III. Multimode Synergy

In this section, we illustrate the multimode synergy in MNZ loop antenna by loading capacitors. To eliminate the influence caused by the metal ground, frame, and back cover, we conduct our discussion in free space. First, we demonstrate a specific case of an ideal multimodal example to validate the correctness of multimode synergy. Second, we introduce our design through parameter analysis, aiming to form a theoretical guide to the design of multimode MNZ antenna.

A. Specified Multimode Case

Fig. 3(a) demonstrates a loop antenna loaded with capacitors in free space. The dimensions of the antenna are $l_a = 43.4$ mm and $w_a = 5.6$ mm. Depending on the capacitor positions, we divide them into two categories. First, capacitor 1 is located at the current nulls of the 1st mode and the 3rd mode. Second, capacitor 2 is located at other current nulls of the 3rd mode. The capacitances of capacitors 1 and 2 are C_1 and C_2, respectively. By setting $C_1 = 0.04$ pF and $C_2 = 0.04$ pF, the simulated S_{11} of the proposed antenna in free space is presented in Fig. 3(b). According to the simulation results, four modes are clearly visible, with a frequency ratio between the highest mode and lowest mode of approximately 1.6. This is much smaller than the usual frequency ratio of 3 between

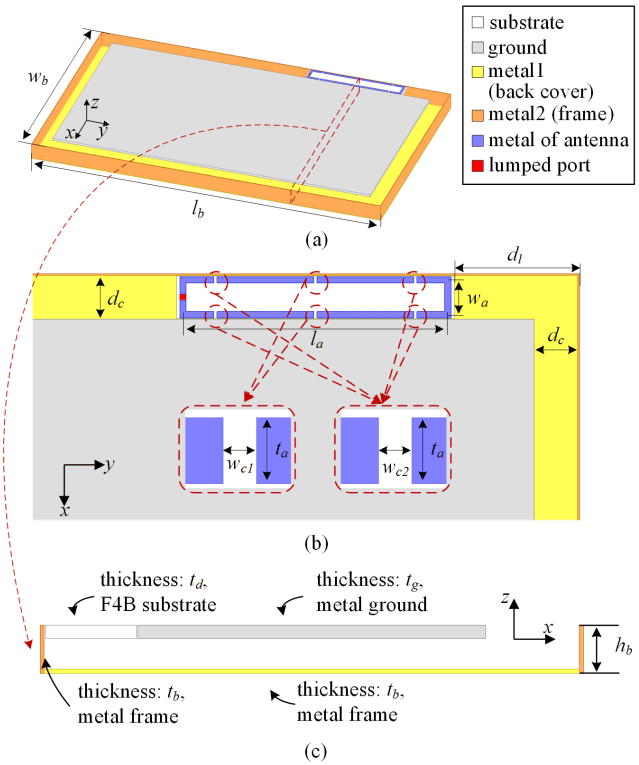

Fig. 2. Antenna geometry of the proposed MNZ loop in a mock-up full metal housing tablet computer. (a) Three-dimensional view. (b) Top view. (c) Side view.

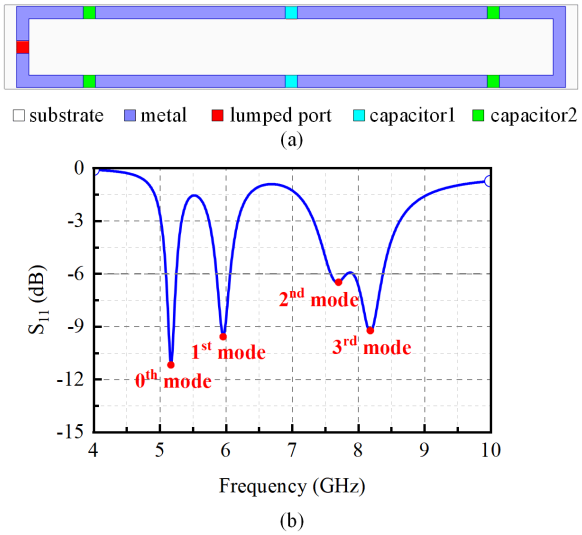

Fig. 3. Design of the multimode loop antenna in free space. (a) Geometry and capacitor parameters assumption of the MNZ loop antenna. (b) Simulated S_{11} and mode distributions of the MNZ loop antenna in free space.

the 3rd mode and the 1st mode in a general loop antenna, demonstrating that we have realized compression among these four modes.

To illustrate the correspondence between the modes on the proposed antenna and the loop antenna without segments, Fig. 4 displays the surface current distributions. In the 0th mode, the surface currents are almost uniform with the same direction and no phase shift, which is identical to that of a small-loop antenna. It is a sign of the establishment of the 0th mode resonance [25], [26]. In the 1st mode, the currents experience two reverses, thus forming two nulls along the

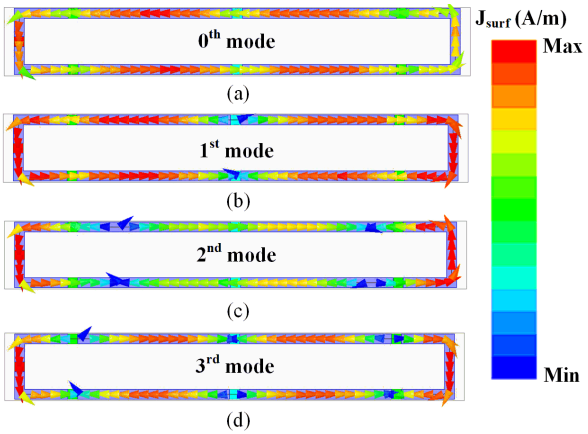

Fig. 4. Simulated surface current distributions of the MNZ loop antenna in free space for (a) 0th mode, (b) 1st mode, (c) 2nd mode, and (d) 3rd mode.

loop. In the 2nd mode, the currents experience four reverses, constructing four nulls. While in the 3rd mode, the reverse times and nulls are six. The current distributions in all modes are as identical to the corresponding modes of a general loop antenna. In other words, we have regulated the frequencies of the four modes on the loop antenna and realized the mode compression by loading capacitors with specific values at different locations, resulting in a multimode synergy effect.

B. Effective Parameter Theory

As depicted in [29], the effective permeability of a transmission line (TL) can be roughly described according to the right- and left-handed (CRLH) TL theory

$$\mu = \frac{Z}{j\omega} = L_R - \frac{1}{\omega^2 C_L} \tag{1}$$

where C_L represents the series capacitance per unit time (in $F\cdot$ m), primarily from our loaded capacitors, and L_R is the series inductance per unit length (in H/m), mainly from the TL in the loop antenna. ω is the angular frequency. After adding series capacitors to the loop antenna, the effective permeability can be adjusted to be smaller than 1, thus stretching the wavelength in the loop antenna and constructing a multimode resonance at a size much larger than the wavelength of the mode. With the increase of the C_L, the resonance frequencies are decreased. Previous work [25], [26] has proven that when $\mu = 0$, the loop has the 0th mode resonance frequency

$$\omega_0 = \frac{1}{\sqrt{L_R C_L}}. \tag{2}$$

To calculate the nth (n = 1, 2, 3, ...) mode frequency on a loop antenna with a given circumference l, we can formulate the following equation by ensuring the electrical dimensions are equal to their physical dimensions:

$$\frac{l}{2n} = \frac{\lambda}{\sqrt{\mu_r}} = \frac{2\pi c}{\sqrt{\varepsilon_0(L_R\omega_n^2 - 1/C_L)}} \tag{3}$$

where $c = 3 \times 10^8$ m/s is the speed of light, $\varepsilon_0 = 8.85 \times 10^{-12}$ F/m is the vacuum permittivity, and ω_n is the resonant frequency of the nth mode. As an illustrative example of the derivation, we select the 0th mode and 1st mode to calculate

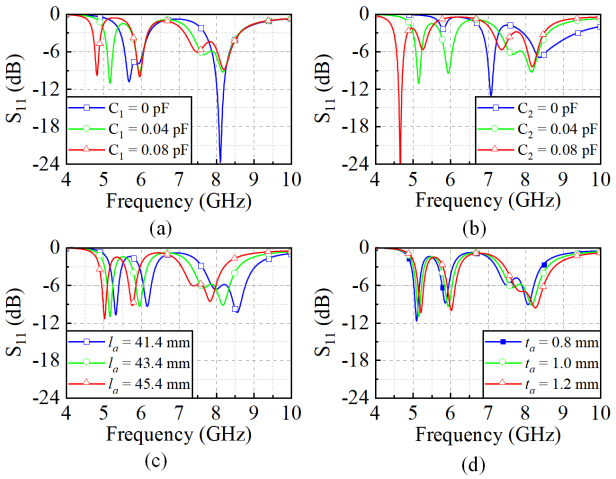

Fig. 5. Analyses of different parameters of the MNZ loop antenna in free space. (a) Changing C_1. (b) Changing C_2. (c) Changing l_a. (d) Changing t_a.

the capacitor values. As depicted in Fig. 3, the resonant frequencies of the 0th mode and 1st mode are equal to $\omega_0 = 2\pi \times 5.17 \times 10^9$ rad/s and $\omega_1 = 2\pi \times 5.96 \times 10^9$ rad/s, respectively. Substituting these values along with equivalent circumference $l = 132.4$ mm into (2) and (3), we obtain a system of two equations with two unknown variables. By solve this system of equations, we find the approximate capacitance and inductance values as $C_L = 5.66 \times 10^{-16}$ F·m and $L_R = 1.68 \times 10^{-6}$ H/m, respectively. As depicted in [29], the real lumped capcatiance and inductance in per unit cell are $C = C_L/d = 0.025$ pF and $L = L_R d = 36.9$ nH, where $d = l/6 = 22$ mm represents the length of per unit cell. Considering both the distributed and lumped capacitance values, the calculated results are essentially consistent with the design, indicating the accuracy of our theory. In summary, through both surface current distributions in Fig. 4 and analyses of different parameters of the MNZ loop antenna in free space in Fig. 5, we will illustrate the specified multimode design from a more engineering point.

C. Design of the Multimode

With the given shape and width of the loop, we have three degrees of freedom to adjust, including the position of the capacitors, the capacitance values, and the length and thickness of the loop. Through the analysis of these parameters, we can draw the following conclusions.

First, placing the capacitors at the positions of the strongest currents in the loop has the most significant effect on stretching the wavelengths. Vice versa, placing the capacitors at the current nulls has little influence of this mode. To prove this conclusion, we compare the current distributions of different modes in Fig. 4. As displayed in Fig. 4(d), the current distribution of the 3rd mode in the segmented loop is almost identical to the regular loop. In other words, the 3rd mode is not stretched. This is because the capacitors are all located at the current nulls of the 3rd mode. In comparison, the wavelengths of the 0th/1st/2nd are apparently stretched because the capacitors are located at the position of the strongest current. Moreover, from Fig. 5(a) and (b), the changes in C_1 and C_2, which are both located at the current nulls of the 3rd mode, have little effect on the frequency of the 3rd mode. Both the current distributions and analyses of parameters illustrate our conclusion regarding the capacitor positions.

Second, with an increase in capacitance, modes shift to lower frequencies. As illustrated in (1) and (3), when the capacitance increases, the permeability decreases with a subsequent decrease in frequency. This phenomenon is also demonstrated in the parameters analyses in Fig. 5. In Fig. 5(a) and (b), when we increase C_1 and C_2, the 0th and the 1st modes, together with the 2nd mode collectively shift to lower frequencies. Simultaneously, the frequency ratio increases, indicating the mode compression. Besides, very small capacitance near the open circuit would make parts of modes unable to be excited. For instance, the 2nd mode is not excited when $C_1 = 0$ pF in Fig. 5(a). This is attributed to the mode current being cut by the open circuit. In a short summary, to achieve mode compression, it is imperative to minimize the capacitance while ensuring the excitation of all modes, facilitating these modes to be as close to each other as possible.

Third, with a change in the loop length and thickness, the modes behave similar to those of complete loop antenna. As depicted in Fig. 5(c) and (d), as the loop length and thickness increasing, all modes shift to lower frequencies. In accordance with these design process, we propose a process for designing a multimode MNZ segmented antenna to cover our desired frequency band: 1) selecting the highest mode to be utilized; 2) calculating the length of the loop antenna, such that the frequency of its highest mode corresponds to the upper limit of the desired frequency band; 3) adding capacitors to the current nulls of all modes; and 4) optimizing the capacitance to enable multimode to coverage across the entire desired frequency band based on our requirements.

TABLE I
SPECIFIC PARAMETER SETTINGS (UNIT: MM)

Parameters	l_b	w_b	l_a	w_a	w_{c1}	w_{c2}	h_b
Size	290	186.5	43.4	5.6	0.5	0.5	7
Parameters	t_a	t_d	t_g	t_b	d_c	d_l	
Size	1	1	1	0.3	7	20	

IV. SIMULATION IN THE MOCK-UP TABLET COMPUTER

In this section, we present and discuss the simulation results of the proposed antenna in the mock-up scenario. After optimizing the parameters in Fig. 2, we obtain the structure with the maximum bandwidth, whose specific dimensions are listed in Table I. Initially, we demonstrate the broadband performance and mode distributions. Subsequently, we discuss the advantages caused by the balanced structure.

A. Broadband Antenna

The simulated S_{11} plot for the proposed antenna is presented in Fig. 6. The $S_{11} < -6$ dB bandwidth spans from 4.5 to 7.5 GHz. The bandwidth covers both 5-GHz (5.15–5.83 GHz) and 6-GHz (5.925–7.125 GHz) bands of Wi-Fi 6/6E. It is noteworthy that the proposed MNZ loop antenna exhibits

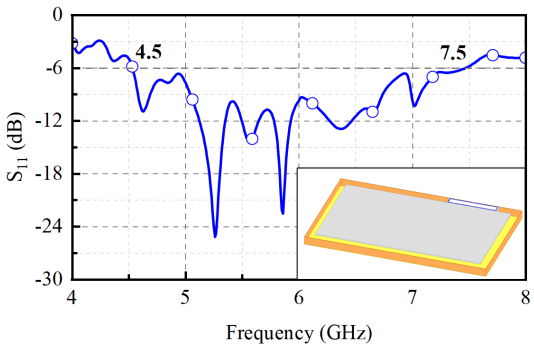

Fig. 6. Simulated S_{11} of the proposed antenna in the mock-up full metal housing tablet computer.

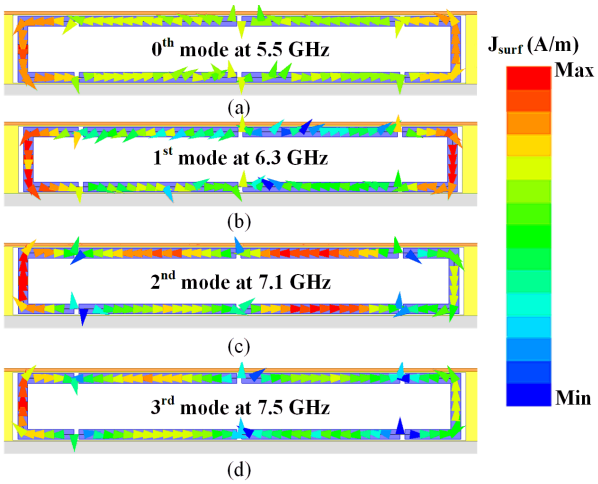

Fig. 7. Simulated surface current distributions of the MNZ loop antenna in the tablet computer scenario for (a) 0th mode at 5.5 GHz, (b) 1st mode at 6.3 GHz, (c) 2nd mode at 7.1 GHz, and (d) 3rd mode at 7.5 GHz.

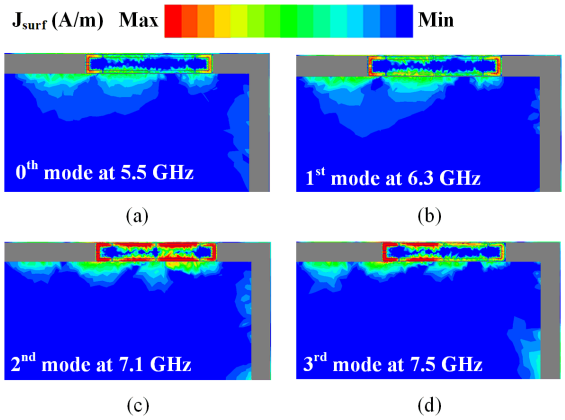

Fig. 8. Simulated surface current distributions of both the MNZ loop antenna and the ground for (a) 0th mode at 5.5 GHz, (b) 1st mode at 6.3 GHz, (c) 2nd mode at 7.1 GHz, and (d) 3rd mode at 7.5 GHz.

superior broadband performance in contrast to its performance in free space. There are two reasons for this enhancement. First, despite the antenna's excitation current being slight, the radiation aperture also increases after introducing the ground. This results in a decrease in the Q-factor for the proposed antenna. Secondly, the metal frame and ground represent two metal segments parallel to the proposed antenna, effectively acting as a shunt capacitor. This shunt capacitor improves impedance matching. In summary, the metal housing increases the radiating aperture, decreases the Q-factor, and acts as a shunt capacitor, leading to a significant improvement in the impedance matching performance.

To further analyze the mode distribution in the mock-up tablet computer, we present the surface current distributions in Fig. 7. In Fig. 7(a), the surface currents become nearly uniform in the same direction at 5.5 GHz, corresponding to the 0th mode. In Fig. 7(b), the surface currents experience two reverses at 6.3 GHz, matching the characteristic of the 1st mode. In Fig. 7(c), the surface currents have four reverses at 7.1 GHz, consistent with the behavior of the 2nd mode. In Fig. 7(d), the surface currents have six reverses at 7.5 GHz, also identical to the 3rd mode. The surface current distributions demonstrate high similarity of the proposed antenna in free space. This illustrates that we achieve broadband performance in the mock-up tablet computer through multimode in the proposed antenna.

B. Advantages Caused by Balanced Structure

As mentioned above, the balanced antennas exhibit little current on the ground and metal housing, thereby possessing the advantages of the robustness on users' hands and cost effectiveness. Modeled after the balanced loop antenna, the proposed MNZ segmented loop antenna also adopts a balanced structure, thereby inheriting these benefits. In Fig. 8, we present the surface current distributions on antenna along with metal ground and frames at four frequencies. It is evident that the currents on the ground are significantly smaller than those on the antenna. In essence, this implies that the loop antenna has minimal impact on the ground, providing direct evidence that the proposed antenna is a balanced structure.

Since the currents on the ground are minimal, the dimensions of the tablet computer theoretically have little impact on the performance of the proposed antenna. As illustrated in Fig. 9, we validate this prediction through the parameter analyses considering both the sizes for tablet computer and relative position for the proposed antenna. As depicted in Fig. 9(a) and (b), the simulated S_{11} exhibits no significant changes in modes when altering the dimensions of the tablet computer. Besides, as Fig. 9(c) demonstrates, the simulated S_{11} also remains nearly constant as the relative position of antenna changes. In other words, benefiting from the balanced antenna, the proposed antenna is suitable for broadband application in full metal housing tablet computer with different dimensions and is hardly affected by the relative position.

Besides, benefiting from the balanced operational modes, the proposed antenna highlights the significant potential of multi-input and multi-output (MIMO) techniques to enhance performance. The schematic of two-element and four-element MIMO is demonstrated in Fig. 10(a) and (b), respectively. As depicted in Fig. 10(c) and (d) (isolations between some elements are omitted owing to the structural symmetry), both systems have an isolation over 10 dB, meeting the requirements of the MIMO techniques. This is attributed to the minimal ground currents excited by the proposed antennas, resulting in almost no mutual coupling and high isolations.

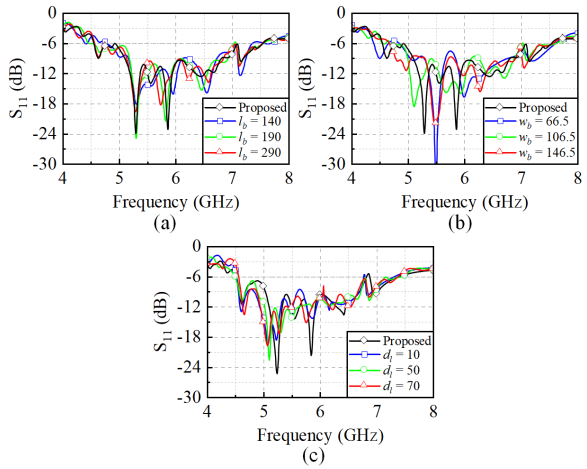

Fig. 9. Parameter analyses for the proposed antenna. (a) Changing l_b. (b) Changing l_a. (c) Changing d_l.

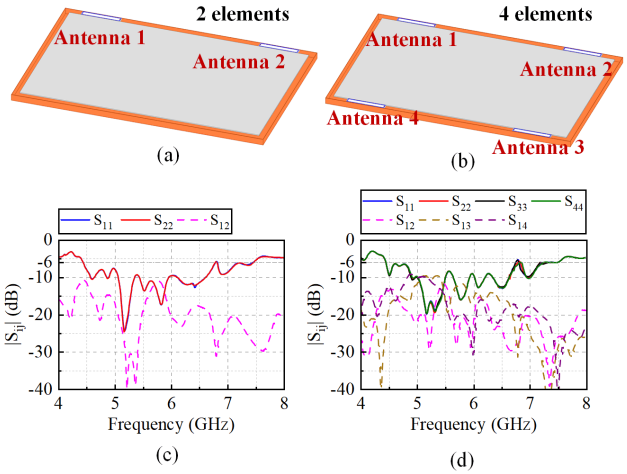

Fig. 10. Simulated reflection coefficients and isolations of the proposed antenna in MIMO cases. (a) Schematic of two-element MIMO. (b) Schematic of four-element MIMO. (c) Simulated S_{ij} in two-element MIMO. (d) Simulated S_{ij} in four-element MIMO.

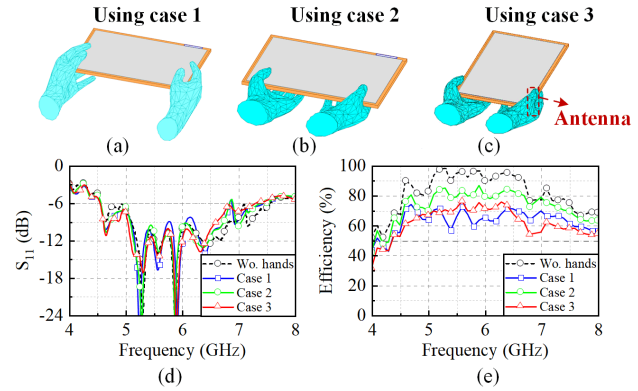

Fig. 11. Simulated S_{11} and efficiencies of the proposed antenna in different practical using cases. (a) Schematic of using case 1. (b) Schematic of using case 2. (c) Schematic of using case 3. (d) Simulated S_{11}. (e) Simulated efficiencies. Wo., without.

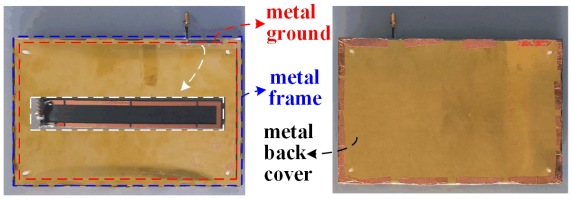

Fig. 12. Photographs of the fabricated in the mock-up full metal housing tablet computer. (a) Top view. (b) Back view.

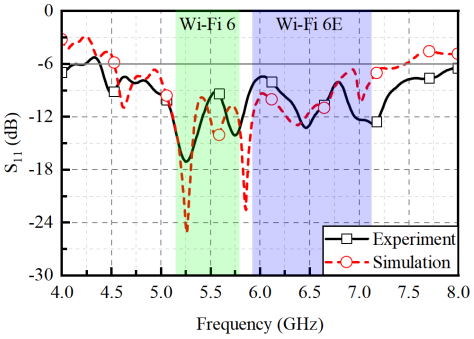

Fig. 13. Measured and simulated S_{11} of the proposed antenna in the mock-up full metal housing tablet computer.

As another additional advantage of the balanced MNZ loop antenna, it appears to be unaffected by the users' hands. Here, we consider three common scenarios for tablet computers, as shown in Fig. 11(a)–(c). These cases include both landscape and portraits modes, even include a case where the hand is covering the antenna in Fig. 11(c). Using predefined hand models in HFSS, we conduct the simulations of S_{11}, along with the efficiency results, and plot them in Fig. 11(d) and (e), respectively. From Fig. 11(c), the results for three scenarios demonstrate nearly identical distributions and bandwidth compared to the proposed antenna without hands. In Fig. 11(e), the simulated efficiencies in practical scenarios decrease due to the losses of the users' hands but remain above 50%. This meets the existing requirements for wireless communication in tablet computers. Benefiting from the balanced structure, the proposed MNZ loop antenna exhibits robust performances in practical scenarios.

V. Experimental Results

In this section, the experimental results are introduced. We have constructed, measured, and discussed a prototype of the proposed antenna, along with a mock-up tablet computer with the dimensions in Table I. The photographs of experimental setups are presented in Fig. 12. The proposed antenna is positioned at the upper right corner of the tablet computer. To excite the antenna, a coaxial cable surrounded by insulating tape is connected to vector network analyzer. A zoomed-in view of the proposed antenna is provided in the inset. The measured S_{11} parameter with simulated result is given in Fig. 13. It can be observed that the measured S_{11} demonstrates broadband characteristics from 4.4 to 8 GHz. The modes in measured S_{11} are in agreement with simulated ones. Cables may introduce losses when the frequency is higher than 7.5 GHz, resulting a decrease in S_{11}. The simulated with measured results cover 5- and 6-GHz band of Wi-Fi 6/6E, validating our design on the multimode MNZ loop antenna.

The simulated and measured radiation patterns are shown in Fig. 14. There are almost no nulls in the radiation patterns, which is beneficial for wireless communication. Additionally,

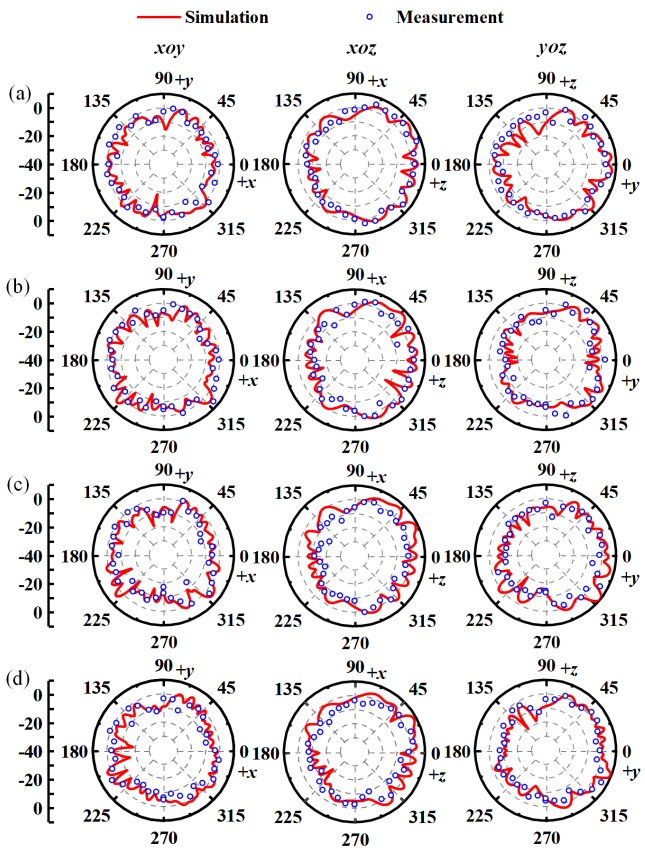

Fig. 14. Simulated and measured 2-D radiation patterns of the proposed antenna at (a) 5.5, (b) 6.3, (c) 7.1, and (d) 7.5 GHz (units: dB).

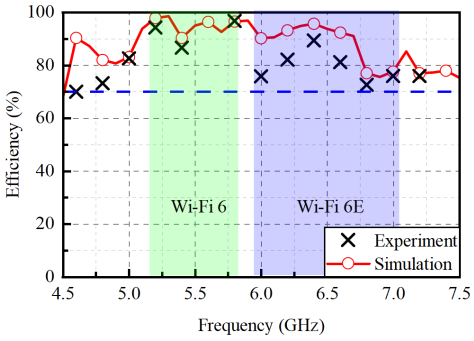

Fig. 15. Measured and simulated efficiencies of the proposed antenna in the mock-up full metal housing tablet computer.

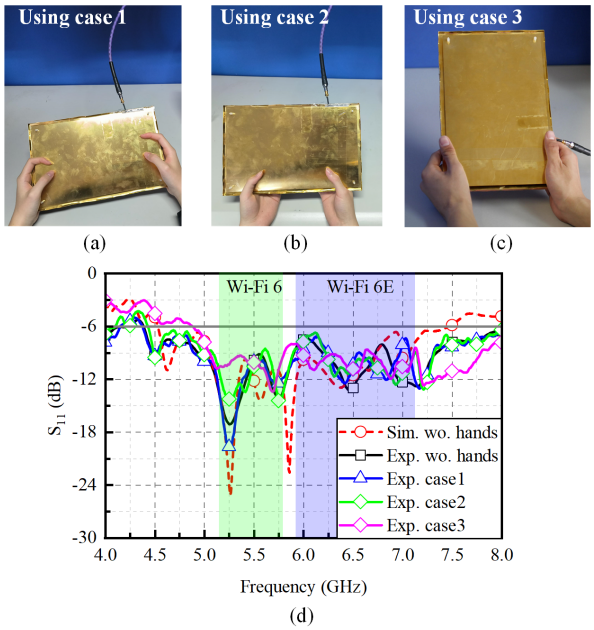

Fig. 16. Measured and simulated S_{11} of the proposed antenna in different practical using cases. (a) Photograph of using case 1. (b) Photograph of using case 2. (c) Photograph of using case 3. (d) Measured and simulated S_{11}.

the measured results correspond well to the simulated ones. The simulated and measured efficiencies of the antenna are shown in Fig. 15. Across the entire frequency band from 4.5 to 7.5 GHz, the measured efficiency consistently remains over 70%. Compared to the simulation results, the measured efficiency decreases in 6–7-GHz band. This is attributed to the increased losses of cables at higher frequencies. As an experimental verification of the simulation regarding to the effects of users' hands, we repeat the using casings in Fig. 10(a)–(c). The photographs of mock-up applications are displayed in Fig. 16(a)–(c), respectively. The measured S_{11} of two different cases, as shown in Fig. 16(d), illustrates the proposed antenna keep the broadband performance covering Wi-Fi 6/6E bands in practical scenarios, even including a case where the hand is covering the antenna. This validates the robustness of the proposed antenna under the effects of users' hands.

To highlight the advantages of the proposed antenna among balanced antennas in the literature, Table II is listed for comparison. Here, λ_0 is the free-space wavelength at the lowest frequency of the operating bandwidth. The antenna proposed in [20] uses a balanced folded loop antenna structure to create the balanced mode and cover the Wi-Fi dual band. However, it receives the limitation on the relative bandwidth and is not available in Wi-Fi 6E applications. The antenna proposed in [26] reaches the dual broad bandwidths, considering using 3-D structure and engraving balanced slots to compromise the integrity of the motherboard. The antennas proposed in [27] and [28] realize the balance through decoupling with the ground and perform well in the isolation for MIMO. However, they have a narrow bandwidth, which cannot satisfy the Wi-Fi 6E band. The antennas proposed in [29] use a T-shape transformer to transfer an unbalanced mode to a balanced mode, requiring relatively large dimensions in the space. Besides, all these antennas are working in free space or mobile terminal devices with dielectric back cover. No cases of balanced antennas in mobile terminals with full metal housing are found in literature research. In this comparison, the proposed MNZ segmented loop antenna realizes the largest relative bandwidth among balanced antennas. Additionally, the proposed antenna is the only one that operates in a tablet computer with full metal housing.

To further illustrate the potential of the proposed antenna in practical applications, the MNZ loop antennas are measured in a real tablet computer with a full metal housing. In order to recreate the application scenarios of the tablet, the antenna is placed in the clearance space, covered by the original glass screen, as depicted in the photographs shown in Fig. 17(a) and (b). The measured S_{11} with efficiency is demonstrated

TABLE II
COMPARISON OF THE PROPOSED ANTENNA AMONG BALANCED ANTENNAS

Ref.	STRUCTURE TYPE (PLANAR/ 3D)	DIMENSIONS* (λ_0^2/λ_0^3)	-6dB Bandwidth (GHz/ %)	Measured efficiency (%)	Antenna type	Full metal housing?
[20]	3D	2.5 × 1.3 × 0.24	2.4 – 2.7 / 11.8 5 – 6 / 18.1	>74	Folded loop	No
[21]	3D	2.5 × 0.5 × 0.19	0.82 – 0.98 / 18 1.7 – 2.4 / 34	>75**	Folded slot	No
[22]	Planar	1.9 × 0.80	3.39 – 3.61 / 6.3	>40	Monopole & slot	No
[23]	Planar	1.7 × 1.48	3.4 – 3.6 / 5.7	>60	Open slot	No
[24]	3D	11 × 0.18 × 0.77	3.3 – 3.8 / 14.1	>42	Transform from IFA to loop	No
Pro.	**Planar**	**6.8 × 1.03**	**4.5 – 7.5 / 50**	**>70**	**MNZ loop**	**Yes**

* Using λ_0^2 for planar structure while λ_0^3 for 3D structure.
**Efficiency is decreased to 25% and 29% when affected by the hand and head, respectively.

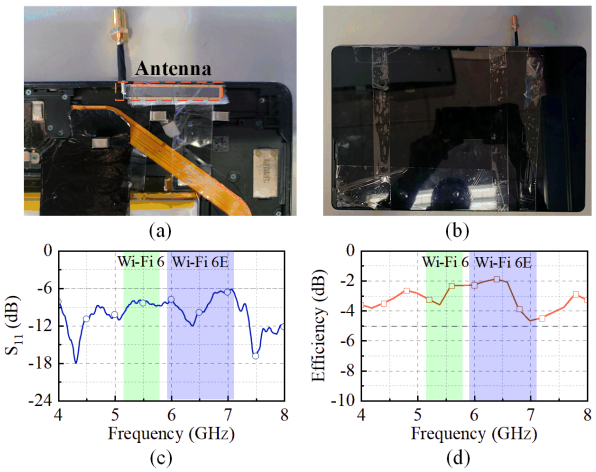

Fig. 17. Measured S_{11} and efficiency of the proposed antenna in real full metal housing tablet computer. (a) Photograph of the tablet computer uncovered by the screen. (b) Photograph of the tablet computer covered by the screen. (c) Measured S_{11}. (d) Measured efficiency.

in Fig. 17(c) and (d), respectively. The measured −6-dB bandwidth is 4–8 GHz, covering two Wi-Fi bands. The lower frequency shift is because of the changes in the dielectric environment. A glass screen spreads over the top view of the proposed antenna, thus enabling the extension of the equivalent electrical size. It leads to the operating band shifting to lower frequency. As displayed in Fig. 17(d), the total efficiency keeps larger than −5 dB. Despite the differences between the simulated and measured results in the mock-up samples, the test results from the real tablet computers meet the requirements for Wi-Fi communication in the industry. This suggests the feasibility of simulating, designing, and testing antennas in a mock-up environment, followed by their integration into real all-metal casing tablets, which holds practical significance for engineering guidance.

VI. CONCLUSION

In this article, we propose a balanced broadband antenna designed for Wi-Fi 6/6E application in a tablet computer with full metal housing. We study the implementation of realizing multiple modes on the segmented loop antenna by loading distributed capacitors and give a generalized approach to design broadband MNZ loop antennas. Through a specific case study, we successfully compress the $0^{th}/1^{st}/2^{nd}/3^{rd}$ modes of the loop. By locating the proposed antenna in the scenario of a mock-up tablet computer with full metal housing, we achieve a broadband covering both 5 and 6 GHz of Wi-Fi 6/6E in a full metal housing tablet computer. Additionally, benefiting from the balanced structure, the proposed antenna exhibits nearly identical performance and mode distributions under different tablet sizes or affecting by hands. The experimental results in the mock-up tablet computer validate the simulation results, and the measured results in a real tablet computer meet the requirements for Wi-Fi 6/6E wireless communication. However, it should be noted that the proposed antenna has a limitation. Due to the balanced modes that do not utilize radiation assistance from the metal ground, its electrical size is larger compared to traditional monopole and invert-F antennas. These balanced modes exclude the influence of the users' hands and head. With sufficient space, the proposed antenna exhibits good performance, which can be applied to real tablet computers. To overcome the limitation, several future works should be undertaken. First, compressing the dimensions of the propose antenna is necessary. Once it can fit into much smaller clearance spaces, the proposed MNZ antenna will be suitable for larger element number MIMO of mobile terminal communication applications. Second, although the existing isolations already meet the MIMO application requirements, we can still increase these through decoupling theories. This is highly beneficial for future integrated MIMO applications. In conclusion, we confirm that the proposed multimode broadband antenna, together with the MNZ antenna design theory, holds significant instructive value for the design of antennas in terminal devices.

REFERENCES

[1] Y. Li, Z. Zhang, Z. Li, J. Zheng, and Z. Feng, "High-permittivity substrate multiresonant antenna inside metallic cover of laptop computer," *IEEE Antennas Wireless Propag. Lett.*, vol. 10, pp. 1092–1095, 2011.
[2] K.-L. Wong and C.-Y. Tsai, "IFA-based metal-frame antenna without ground clearance for the LTE/WWAN operation in the metal-casing tablet computer," *IEEE Trans. Antennas Propag.*, vol. 64, no. 1, pp. 53–60, Jan. 2016.

[3] K. Wong and C. Tsai, "Half-loop frame antenna for the LTE metal-casing tablet device," *IEEE Trans. Antennas Propag.*, vol. 65, no. 1, pp. 71–81, Jan. 2017.

[4] K.-L. Wong, "Planar antennas for wireless communications," *Microw. J.*, vol. 46, no. 10, pp. 144–145, 2003.

[5] C.-Y. Tsai and K.-L. Wong, "Inverted-F antenna-based on-frame GPS/WLAN antenna for the metal-casing tablet computer," in *Proc. 10th Eur. Conf. Antennas Propag. (EuCAP)*, Apr. 2016, pp. 1–4.

[6] S.-C. Chen, C.-C. Huang, and W.-S. Cai, "Integration of a low-profile, long-term evolution/wireless wide area network monopole antenna into the metal frame of tablet computers," *IEEE Trans. Antennas Propag.*, vol. 65, no. 7, pp. 3726–3731, Jul. 2017.

[7] P. Chen, P. Wang, G. Yang, and C. Y. D. Sim, "A compact tri—Band antenna at GPS and WLAN a/b/g frequencies for tablet with full metal housing," in *Proc. IEEE Int. Symp. Antennas Propag. (APSURSI)*, Jun. 2016, pp. 2165–2166.

[8] J.-H. Chou, J.-F. Chang, D.-B. Lin, H.-J. Li, and T.-L. Wu, "A compact loop-slot mode combination antenna for ultra-thin tablet computer with metallic bottom cover," *IEEE Antennas Wireless Propag. Lett.*, vol. 13, pp. 746–749, 2014.

[9] K.-L. Wong and C.-Y. Huang, "Triple-wideband open-slot antenna for the LTE metal-framed tablet device," *IEEE Trans. Antennas Propag.*, vol. 63, no. 12, pp. 5966–5971, Dec. 2015.

[10] Y. Li, Z. Zhang, J. Zheng, Z. Feng, and M. F. Iskander, "A compact hepta-band loop-inverted f reconfigurable antenna for mobile phone," *IEEE Trans. Antennas Propag.*, vol. 60, no. 1, pp. 389–392, Jan. 2012.

[11] Y. Li, Z. Zhang, J. Zheng, and Z. Feng, "Compact heptaband reconfigurable loop antenna for mobile handset," *IEEE Antennas Wireless Propag. Lett.*, vol. 10, pp. 1162–1165, 2011.

[12] M. Hu and Y. Li, "Wideband back cover microstrip antenna with multiple shorting vias for mobile 5G MIMO applications," *IEEE Trans. Antennas Propag.*, vol. 71, no. 10, pp. 8290–8295, Oct. 2023.

[13] C. Deng, Y. Li, Z. Zhang, and Z. Feng, "A novel low-profile hepta-band handset antenna using modes controlling method," *IEEE Trans. Antennas Propag.*, vol. 63, no. 2, pp. 799–804, Feb. 2015.

[14] C. Deng, Y. Li, Z. Zhang, and Z. Feng, "Planar printed multi-resonant antenna for octa-band WWAN/LTE mobile handset," *IEEE Antennas Wireless Propag. Lett.*, vol. 14, pp. 1734–1737, 2015.

[15] W. Sun, Y. Li, L. Chang, H. Li, X. Qin, and H. Wang, "Dual-band dual-polarized microstrip antenna array using double-layer gridded patches for 5G millimeter-wave applications," *IEEE Trans. Antennas Propag.*, vol. 69, no. 10, pp. 6489–6499, Oct. 2021.

[16] Y. Zhang, Y. Li, W. Zhang, Z. Zhang, and Z. Feng, "Omnidirectional antenna diversity system for high-speed onboard communication," *Engineering*, vol. 11, no. 4, pp. 72–79, Apr. 2022.

[17] Y. Zhang and Y. Li, "Wideband microstrip antenna in small volume without using fundamental mode," *Electromagn. Sci.*, vol. 1, no. 2, 2023, Art. no. 0020073.

[18] C. Shen, W.-J. Lu, and L. Zhu, "Planar self-balanced magnetic dipole antenna with wide beamwidth characteristic," *IEEE Trans. Antennas Propag.*, vol. 67, no. 7, pp. 4860–4865, Jul. 2019.

[19] K.-D. Hong, X. Zhang, L. Zhu, X.-K. Bi, Z. Chen, and T. Yuan, "A self-balanced wideband patch antenna fed with a U-resonator for stable radiation performance," *IEEE Antennas Wireless Propag. Lett.*, vol. 19, pp. 661–665, 2020.

[20] A. G. Alhaddad, R. A. Abd-Alhameed, D. Zhou, C. H. See, P. S. Excell, and S. M. R. Jones, "Folded loop balanced coplanar antenna for WLAN applications," *IEEE Trans. Antennas Propag.*, vol. 60, no. 10, pp. 4916–4920, Oct. 2012.

[21] S. Heun Lee, Y. Lim, Y. Joong Yoon, C.-B. Hong, and H.-I. Kim, "Multiband folded slot antenna with reduced hand effect for handsets," *IEEE Antennas Wireless Propag. Lett.*, vol. 9, pp. 674–677, 2010.

[22] L. Chang, Y. Yu, K. Wei, and H. Wang, "Orthogonally polarized dual antenna pair with high isolation and balanced high performance for 5G MIMO smartphone," *IEEE Trans. Antennas Propag.*, vol. 68, no. 5, pp. 3487–3495, May 2020.

[23] Y. Li, C.-Y.-D. Sim, Y. Luo, and G. Yang, "High-isolation 3.5 GHz eight-antenna MIMO array using balanced open-slot antenna element for 5G smartphones," *IEEE Trans. Antennas Propag.*, vol. 67, no. 6, pp. 3820–3830, Jun. 2019.

[24] J. Sui, C. Huang, and Y.-F. Cheng, "Multi-element fully decoupled inverted-F antennas for mobile terminals," *IEEE Trans. Antennas Propag.*, vol. 70, no. 11, pp. 10076–10085, Nov. 2022.

[25] K. Wei, Z. Zhang, Z. Feng, and M. F. Iskander, "A MNG-TL loop antenna array with horizontally polarized omnidirectional patterns," *IEEE Trans. Antennas Propag.*, vol. 60, no. 6, pp. 2702–2710, Jun. 2012.

[26] K. Wei, Z. Zhang, and Z. Feng, "Design of a wideband horizontally polarized omnidirectional printed loop antenna," *IEEE Antennas Wireless Propag. Lett.*, vol. 11, pp. 49–52, 2012.

[27] K. Wei, Z. Zhang, Z. Feng, and M. F. Iskander, "A wideband MNG-TL dipole antenna with stable radiation patterns," *IEEE Trans. Antennas Propag.*, vol. 61, no. 5, pp. 2418–2424, May 2013.

[28] H. Li and Y. Li, "Mode compression method for wideband dipole antenna by dual-point capacitive loadings," *IEEE Trans. Antennas Propag.*, vol. 68, no. 8, pp. 6424–6428, Aug. 2020.

[29] J.-H. Park, Y.-H. Ryu, and J.-H. Lee, "Mu-zero resonance antenna," *IEEE Trans. Antennas Propag.*, vol. 58, no. 6, pp. 1865–1875, Jun. 2010.

Wendi Yan (Graduate Student Member, IEEE) received the B.S. degree in electronic engineering from Tsinghua University, Beijing, China, in 2021, where he is currently pursuing the Ph.D. degree in electronic engineering.

His current research interests include terminal antennas, metamaterial antennas, epsilon-near-zero antennas, and mu-near-zero antennas.

Yongjian Zhang received the B.S. degree in communication engineering from Tongji University, Shanghai, China, in 2018, and the Ph.D. degree in electronic engineering from Tsinghua University, Beijing, China, in 2023.

He is currently a Post-Doctoral Fellow with the Department of Electronic Engineering, Tsinghua University. His current research interests include aircraft antennas, dual-polarized antennas, and multiple-input and multiple-output (MIMO) antenna arrays.

Dr. Zhang serves as a reviewer for the IEEE TRANSACTIONS ON ANTENNAS AND PROPAGATION, IEEE ANTENNAS AND WIRELESS PROPAGATION LETTERS, and *Microwave and Optical Technology Letters*.

Kaifeng Li is currently pursuing the B.S. degree in electronic engineering from Tsinghua University, Beijing, China.

His current research interests include wideband antennas, metamaterial antennas, and microstrip antennas.

Hui Lin received the B.S. and M.S. degrees from the University of Science and Technology of China, Hefei, China, in 2003 and 2006, respectively.

He is currently with Lenovo Group, Shanghai, China. His research interests include antennas, RF components, and tablet hardware systems.

Heng Guo received the B.S. and M.S. degrees in electronic and information engineering from Beihang University, Beijing, China, in 2006 and 2009, respectively.

He is currently with Lenovo Group, Beijing. His research interests include small antenna, circularly polarized antenna, and smart antenna.

Shumin Liao received the B.E. degree from Hubei Normal University, Hubei, China, in 2017, and the M.S. degree in information and communication engineering from Shenzhen University, Shenzhen, China, in 2020.

She is currently an Antenna Engineer with the Tablet Business Department, Lenovo Group Ltd., Shanghai, China. Her current research interests include the development and application of mobile terminal antennas.

Yue Li (Senior Member, IEEE) received the B.S. degree in telecommunication engineering from Zhejiang University, Hangzhou, Zhejiang, China, in 2007, and the Ph.D. degree in electronic engineering from Tsinghua University, Beijing, China, in 2012.

In June 2012, he was a Post-Doctoral Fellow with the Department of Electronic Engineering, Tsinghua University. In December 2013, he was a Research Scholar with the Department of Electrical and Systems Engineering, University of Pennsylvania, Philadelphia, PA, USA. He was also a Visiting Scholar with the Institute for Infocomm Research (I2R), A∗STAR, Singapore, in 2010, and Hawaii Center of Advanced Communication (HCAC), University of Hawaii at Manoa, Honolulu, HI, USA, in 2012. Since January 2016, he has been with Tsinghua University, where he is currently an Assistant Professor and an Associate Professor with the Department of Electronic Engineering. He has authored and coauthored over 210 journal articles and 50 international conference papers. He holds 26 granted Chinese patents. His current research interests include metamaterials, plasmonics, electromagnetics, nanocircuits, mobile and handset antennas, MIMO and diversity antennas, and millimeter-wave antennas and arrays.

Dr. Li was a recipient of the Issac Koga Gold Medal from URSI General Assembly in 2017, the Second Prize of Science and Technology Award of China Institute of Communications in 2017, the Young Scientist Award from the conferences of Progress in Electromagnetics Research Symposium (PIERS) in 2019, the International Applied Computational Electromagnetics Society Symposium (ACES) in 2018, the Atlantic Radio Science Conference (AT-RASC) in 2018, the Asia–Pacific Radio Science Conference (AP-RASC) in 2016, the International Symposium on Electromagnetic Theory (EMTS) in 2016, and the URSI General Assembly and Scientific Symposium (GASS) in 2014; the Best Paper Award from the conferences of Photonics and Electromagnetics Research Symposium (PIERS) in 2021, the International Workshop on Electromagnetics (iWEM) in 2021, the Asia–Pacific Conference on Antennas and Propagation (APCAP) in 2017 and 2020, the U.K.-Europe-China Workshop on Millimeter Waves and Terahertz Technologies (UCMMT) in 2020, the International Symposium on Antennas and Propagation (ISAP) in 2019, the Cross Strait Quad-Regional Radio Science and Wireless Technology Conference (CSQRWC) in 2018, the International Symposium on Antennas, Propagation and EM Theory (ISAPE) in 2016 and 2021, the International Conference on Microwave and Millimeter Wave Technology (ICMMT) in 2016 and 2020, the National Conference on Microwave and Millimeter Waves (NCMMW) in 2017 and 2018, and the National Conference on Antennas (NCANT) in 2017 and 2019; the Outstanding Doctoral Dissertation of Beijing Municipality in 2013; and the Principal Scholarship of Tsinghua University in 2011. He is serving as an Associate Editor for the IEEE TRANSACTIONS ON ANTENNAS AND PROPAGATION, IEEE ANTENNAS AND WIRELESS PROPAGATION LETTERS, *Microwave and Optical Technology Letters*, and *Computer Applications in Engineering Education*. He is also serving on the Editorial Board for *Scientific Reports*, *Sensors*, and *Electronics*.